



## Research article

# Investigation of structural, mechanical, electronic and optical responses of Ga doped aluminum arsenide for optoelectronic applications: By first principles

Anwar Ali<sup>a</sup>, Abdul Waheed Anwar<sup>a,\*</sup>, Muhammad Moin<sup>a,b,\*\*</sup>, Mehrunisa Babar<sup>a</sup>, Udayabhaskararao Thumu<sup>b</sup>

<sup>a</sup> Department of Physics, University of Engineering and Technology, Lahore, Pakistan

<sup>b</sup> Institute of Fundamental and Frontier Sciences, University of Electronic Science and Technology of China, Chengdu, 610054, China

## ARTICLE INFO

## Keywords:

Aluminium gallium arsenide  
Refractive index  
Band gap engineering  
Specific heat  
Bulk modulus  
Born stability

## ABSTRACT

Owing to the rapidly increasing performance of ternary semiconductors; Aluminium Gallium Arsenide ( $\text{Al}_{1-x}\text{Ga}_x\text{As}$ ;  $x = 0, 0.25, 0.50, 0.75$ ) has been studied by first-principles calculations in Cambridge Serial Total Energy Package (CASTEP-Code). Density functional theory in the frame of full potential linear augmented plane wave (FP-LAPW) is used. The structural, electronic, and optical behavior of the Zinc Blend (ZB) structure of AIAs with Ga impurity was computed by using generalized gradient approximation (GGA) as exchange potential and Perdew-Burke-Ernzerhof (PBE) as functional. Changes in lattice parameters (a), bulk modulus (66.07–76.85), hardness (5.79–8.91) and machinability (1.36–1.46), band gap energy ( $E_g$ ), and optical properties are computed and discussed in this work. Lattice parameters and elastic constants showed excellent agreement with the reported data whereas some properties were found to excel much more than the theoretical reports. Remarkable bandgap reduction from 1.7eV to 0.28eV is very encouraging in its low-energy applications in UV and visible ranges. Real (Re) and Imaginary (Im) parts of the dielectric function and refractive index shifts towards lower energy values show good agreement with those of theoretical and experimental works. We contribute to the knowledge and characterization of  $\text{Al}_{1-x}\text{Ga}_x\text{As}$  facilitating its integration into various technological advancements such as photovoltaic, laser, diodes, and high-frequency transistors.

## 1. Introduction

Incorporation of impurity in a material is a highly favorite technique to design the structure which creates ionizability inside the material. This is found to be a healthy approach in research and laboratory work for tailoring of semiconductors [1]. In this context, important concepts are; the two types of carriers, electrons and holes, energy band and the way how to control carrier concentrations by impurities. In a pure semi-conductor, there is a gap between valence band and conduction band. Where electrons reside and cannot move freely is called valence band having lower energy value comparative to the conduction band where electron is free to move as a charge carrier. This gap classify the semiconductors as electrical insulators. This case is not only for elemental semiconductors but may

\* Corresponding author.

\*\* Corresponding author. Department of Physics, University of Engineering and Technology, Lahore, Pakistan.

E-mail addresses: [abdulwaheedanwar@uet.edu.pk](mailto:abdulwaheedanwar@uet.edu.pk) (A.W. Anwar), [moingcs786@gmail.com](mailto:moingcs786@gmail.com) (M. Moin).

<https://doi.org/10.1016/j.heliyon.2024.e24597>

Received 14 August 2023; Received in revised form 10 January 2024; Accepted 10 January 2024

Available online 17 January 2024

2405-8440/© 2024 Published by Elsevier Ltd.

This is an open access article under the CC BY-NC-ND license

(<http://creativecommons.org/licenses/by-nc-nd/4.0/>).

even be demanding for binary or ternary compounds as well. At the commercial level it is highly demanding to reduce this gap so we can get sufficient electrical conductivity from this class of materials [2]. Incorporation of impurity in to the single Fermi-level and Fermi distribution function are very valuable facts and tools. Fermi-level is closely linked to the concentrations of electrons and holes inside the material. Compounds of Aluminium and Arsenic have been explored by different methods in numerous experimental and theoretical studies. Material explored in this computational work is Aluminium Arsenide (AlAs); Aluminium (Al) from III-group and Arsenic (As) from the V-group and Gallium (Ga) the impurity from III group. Binary semiconductor material AlAs have nearly the same lattice parameters as that of intrinsic GaAs with Zinc Blend structure [3]. Layers of AlAs have very little induced strains which allows high electron mobility potentially making them very essential for a number of high speed electronics and opto-electronic devices. It is highly important to enhance the probability of electron occupancy at different energy levels [4,5]. Compounds with III-group elements are characterized in terms of high electron mobility, low carrier concentrations even with a good thermal stability. Ternary alloys of AlAs with III group elements has gained tremendous attention over the recent years as it has the largest applications in the field of electronics and optoelectronic devices [6]. We noted that theoretical studies have not yet been reported uniquely about  $\text{Al}_x\text{Ga}_{1-x}\text{As}$  in which AlAs is as pristine and Ga is the impurity [7]. These materials can determinately be applied in very high speed digital: microwaves of high-frequencies, LEDs, LASER diodes, high electron mobility transitions and electro-optic devices due to their excellent miscibility and high carrier mobility [7,8]. Closer the CB to the Fermi level, it will easier for electrons to jump into the CB. This shift provides a cause of better understanding and its utilization of a very big class of materials that is semiconductors which are at the front panel among all such choices of shift. The insertion of carriers that transit photo-excitations are outstanding in their throughput in optical devices [9]. The successful addition of a semiconductor for the III group, like the classic Ga in AlAs is generally a unique event for the ambipolar doping of both the n-type (electrons) and p-type (holes) [10]. Aluminum Arsenide with Zinc blend crystal structure has a lattice parameter 5.66 Å [11]. A clear and dedicated path is adopted in this work to elaborate the most desired aspects of  $\text{Al}_{1-x}\text{Ga}_x\text{As}$  with the enhanced value of Ga ( $x = 0$  to 0.75) as a well potential candidate in the ultraviolet UV spectrum as a photodetector [11]. The effective predicted changes are; first is the shift of Fermi level either toward the conduction band or valence band due to its impressive doping into degenerated n-type or p-type semiconductors. The second one is the introduction of mid bandgap which permits many wavelengths absorption and hence changed the bandgap values by gallium [12]. Followings are the three chemical combination comprising of; Al-rich (Ga-poor), Al-moderate (Ga-moderate) and Al-poor (Ga-rich) are considered. Comparative to the intrinsic defects, the extrinsic material may show prominent effect on the properties of the material [13]. The property parameters of  $\text{Al}_{1-x}\text{Ga}_x\text{As}$  like formation as well as transition energies have not yet been explored. A systematic study of AlAs is needed for deep consideration of electronic and optical achievements of ternary semiconductors. It has been observed by literature that there have been very much suitable methods; empty space diffusion, inner diffusion of lattice, and change of places to alter Ga atom concentration in pure AlAs to form new ternary material [14]. Computational material science is the best method to unravel the hidden structural properties of the material, especially on a single plate form. Density functional theory (DFT) uses the linear augmented plane wave (LAPW) method to analyze structural, electronic and optical properties [15]. Several computer programs are governing the DFT but the present calculations are computed by CASTEP-Code built in the material studio. Structural parameters like lattice constants, phases, a special distribution of atoms, and moduli are analyzed by (GGA-PBESol) [16]. The calculations by First-principles are based on DFT and compute one of the highly accurate microscopic theories in material science [17].

## 2. Theoretical discussion

To define the whole molecule as a motion group of all atoms, a molecule is described by a single set of translational and rotational parameters. The first principles calculations demonstrate properties of the materials at the most stable state i-e the ground state at which the characteristics of many-electron systems are determined by the density of electrons depending only on 3N-spatial coordinates reduces to 3-spatial coordinates. *Atomic observables that describe the atom or molecules, termed as its gradients.* Relative to local density approximation (LDA), the generalized gradient approximation (GGA) produces effective results that strengthen the experimental research work. DFT works at the ground state so all computations can only be performed for the density  $[n(r)]$  at the ground state. By this concept, Hohenberg and Kohn prove the energy functional  $E[n(r)]$  [18]. Ground state density  $[n(r)]$  produces the most reliable response of the material. Henceforth, these were the results that enabled Hohenberg and Kohn to lead the derivation of energy functional of the density  $E[n(r)]$  from the Hamiltonian,

$$H = - \sum_i \frac{\hbar^2}{2m_e} \nabla_{r_i}^2 + \sum_i V_{ext}(r_i) + \frac{e^2}{2} \sum_{i \neq j} \frac{1}{|r_i - r_j|} + \sum_{i \neq j} \frac{Z_i Z_j e^2}{|R_i - R_j|} \quad (1)$$

In actuality, the results of Kohn Sham relations give the true energy at the ground state which assumes lowest value of the interacting electrons gas system.

$$E[n(r)] = \int V_{ext}(r)n(r)dr + F[n(r)] \quad (2)$$

However, for inhomogeneous interacting electrons, the adopted approximation is GGA [19],

$$E_{XC}[n(r)] = \int \epsilon_{XC}(r)n(r)dr \quad (3)$$

$E_x$  is the exchange co-relation energy of the system.

### 3. Computational detail

Computational material science is the best method to unravel the hidden properties. The progress in high accuracy and efficiency of calculations plays a vital role in the verification of material with its properties [20]. *Atomic observables that describe the atom or molecules, termed as its gradients.* To define the whole molecule as a motion group of all atoms, a molecule is described by a single set of translational and rotational parameters [21]. DFT represents very accurate microscopic theories in material science. Several computer programs are governing the DFT but we have used the Cambridge Serial Total Energy Package (CASTEP) Code by the scheme of generalized gradient approximation (GGA) with the functional PBESol (Perdew–Burke–Ernzerhof) [22]. All studies must be performed on a periodic system, even when the periodicity is superficial, that's why CASTEP-code is used for a supercell method which ensures the behavior of material on the whole [23]. This code creates faster and easier calculations which enhance efficiency. The structural, electronic and optical trends are computed by GGA. Comparative to LDA, GGA-PBE gives very accurate results which guarantee the experimental research work [21]. To examine the material  $\text{Al}_{1-x}\text{Ga}_x\text{As}$  for its structural, electronic, and optical properties, the followings are the computational settings. Calculations were performed by conventional DFT settings at the temperature of 0 K. A super cell of  $1 \times 1 \times 1$  was created. In a manner, to get the exact answer the absolute number of functions are required therefore cut-off have to be introduced to get definite results. Therefore, the total cut-off energy for the plane wave basis was set as 420 eV. The Monkhorst–Pack scheme of K-points grid sampling was set as  $8 \times 8 \times 8$  for the irreducible first Brillouin Zone. The minimization algorithm chosen was the Broyden–Fletcher–Goldfarb–Shanno (BFGS) scheme [24]. In computational work. Augmented wave base converging pseudopotentials are employed to access the ion and electron interaction. The criterion of convergence was set by the layout as; less than 0.03 eV/Å was the force on the atoms, less than 0.03 GPa was the stress on the atoms, less than 0.001 Å was the atomic displacement and  $1.0 \times 10^{-5}$  eV was the energy change per atom [25]. For the computation of properties of materials, the convergence condition of total associated energy in a self-consistent field is very important. All results for  $\text{Al}_{1-x}\text{Ga}_x\text{As}$  ( $x = 0, 0.25, 0.50, 0.75$ ) were computed with these settings to get reliable optimized crystal structures. Knowledge of computation for structural values permits the unit cell volume evolution for the crystal structure in the semiconductors. Results are consistent with the recent experimental and computed data.

### 4. Results and discussions

#### 4.1. Structural properties

The most stable structure of molecule by its formation energy is at the ground state which is calculated by Birch Murnaghan's approach with GGA-PBESol changing total energy at different volumes along the equilibrium cell volume.

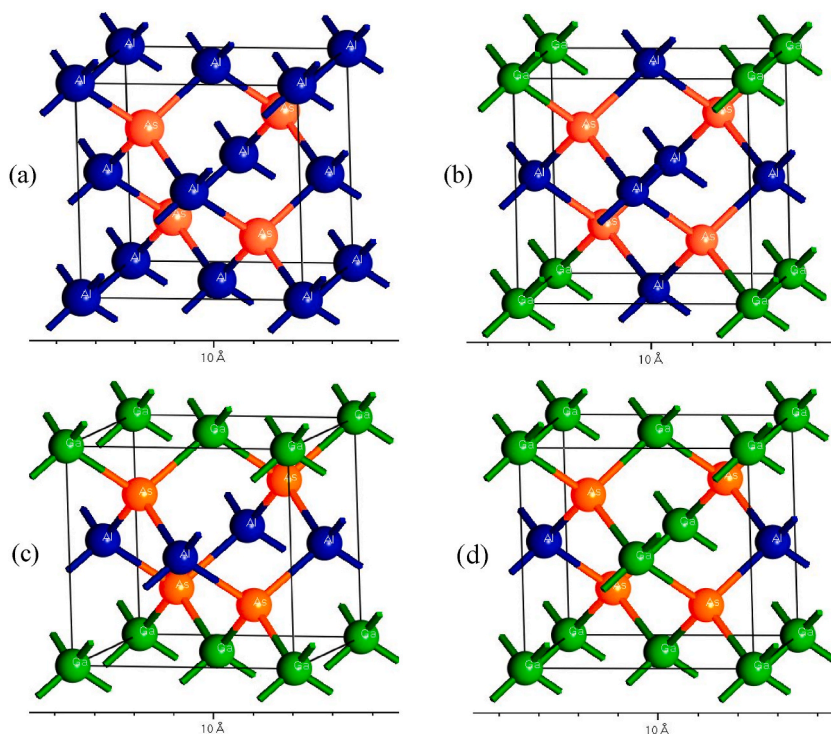


**Fig. 1.** Optimized Structures of (a) pure AlAs (b)  $\text{Al}_{0.75}\text{Ga}_{0.25}\text{As}$  (c)  $\text{Al}_{0.50}\text{Ga}_{0.50}\text{As}$  (d)  $\text{Al}_{0.25}\text{Ga}_{0.75}\text{As}$ .

$$E(V) = E_o + \frac{B_o V}{B'_o} \left( \frac{(V_o/V)^{B'_o}}{B'_o - 1} + 1 \right) - \frac{B_o V_o}{B'_o - 1} \quad (4)$$

Where,  $B_o$  is bulk modulus,  $V_o$  is the reference volume at zero pressure of the scheme,  $V$  is a deformed volume of the unit cell and  $B'_o$  is the derivative of the bulk modulus [25]. To assess stability of our material, we calculated the formation energy  $E_f$  by using;

$$E_{\text{form}}(x) = E_{\text{total}} - \sum X E_{\text{total}}(x) \quad (5)$$

$E_x$  is the total energies of the pristine AlAs,  $E_{\text{form}}$  is the dissociation energy of the molecule into its components [26].

It is worth pointing out here that the  $E_{\text{xc}}$  and  $V_{\text{xc}}$  parts are computed using the GGA-PBESol. The ZB structure of AlAs has cubic space group F-43m (face-centered cubic lattice) in which the position of Al is at (0, 0, 0) and (0.25, 0.25, 0.25) while As is at interstitial place (0.25, 0.25, 0.25) as shown in Fig. 1(a-d) [27].

Optimized volume of structure was obtained by plotting the unit cell volume against total energy. Calculated convergence energy value for Al is  $-6603.782$  eV whereas it is  $-61519.637$  eV for As. Volume of constructed cell was  $181.53 \text{ \AA}^3$  and volume of optimized cell is  $183.21 \text{ \AA}^3$ . In this context, obtained lattice constants and volume at the least values of crystal total energy  $E_o$  for intrinsic (AlAs) and doped structures at concentrations,  $x = 0.25, 0.50, 0.75$  ( $\text{Al}_{1-x}\text{Ga}_x\text{As}$ ) were obtained, shown in Fig. 1(a) and Fig. 1(candd), respectively. By the impact of Ga into the AlAs at the place of Al, the lattice values changes according to the strength of the dopant as obvious from the trends in Fig. 2 (a,b). This small difference in lattice parameters is due to the difference of ionic radii of the elements with different concentrations. Lattice constants increases due to increase in atomic number while the bulk modulus decreases due to shielding effect. Greater cell volume provides more space for states to overlap with least energy which in turn is in favor of band formation with large density of states [28]. Our calculated values are in decent agreement with the experimental values. The ground-state parameters along with: experimental and theoretical values are listed in Table 1.

Experimentally reported pristine AlAs structure has each of its crystal angles at  $90^\circ$  with bulk modulus 82.02 GPa and structural formation  $\Delta H_f$  is  $-19821.90$  eV. In this computed research work the pure optimized AlAs has maintained its each crystal angles at  $90^\circ$  with the enhanced value of its bulk modulus 85.15 GPa with the change of 3.13 GPa which shows the strength of our material to bear more stresses under the same physical conditions. This is because of the increased value of formation energy of the unit cell (AlAs). In the case of ternary  $\text{Al}_{0.75}\text{Ga}_{0.25}\text{As}$ , the crystal angle  $\beta$  varies briefly to new value at  $89.99^\circ$  with the reduced value of its bulk modulus to 71.34 GPa with the net change of 10.67 GPa which shows the shielding effect of electron due to the involvement of new states of Ga atoms. This is because of the increased value of formation energy of the unit cell (AlAs). For  $\text{Al}_{0.50}\text{Ga}_{0.50}\text{As}$ , the crystal angle  $\beta$  varies briefly to new values at  $89.99^\circ$  with the significant enhanced value of its bulk modulus to 97.13 GPa with the formation energy value of  $-16373.33$  eV which encourages to its stress-strain durability. And finally,  $\text{Al}_{0.25}\text{Ga}_{0.75}\text{As}$  showed lesser bulk modulus of 42.45 GPa along with the formation energy value of  $-18410.60$  eV. The values of structural orientations with the negligible change and information of the pure and  $\text{Al}_{1-x}\text{Ga}_x\text{As}$  ( $x = 0.25, 0.50, 0.75$ ) are shown in Table 2 with the supportive information. The material is mechanically stable by the introduction of Ga in AlAs.

The essence of the work is suitable with the computed and experimental data values and are in good interface for its reliability in the field of electronics, LEDs, LASER diodes, high electron mobility transitions and electro-optic devices.

#### 4.2. Elastic constants

Elastic calculations provide the bonding character between neighboring atomic planes, the anisotropic response of bonding, in-

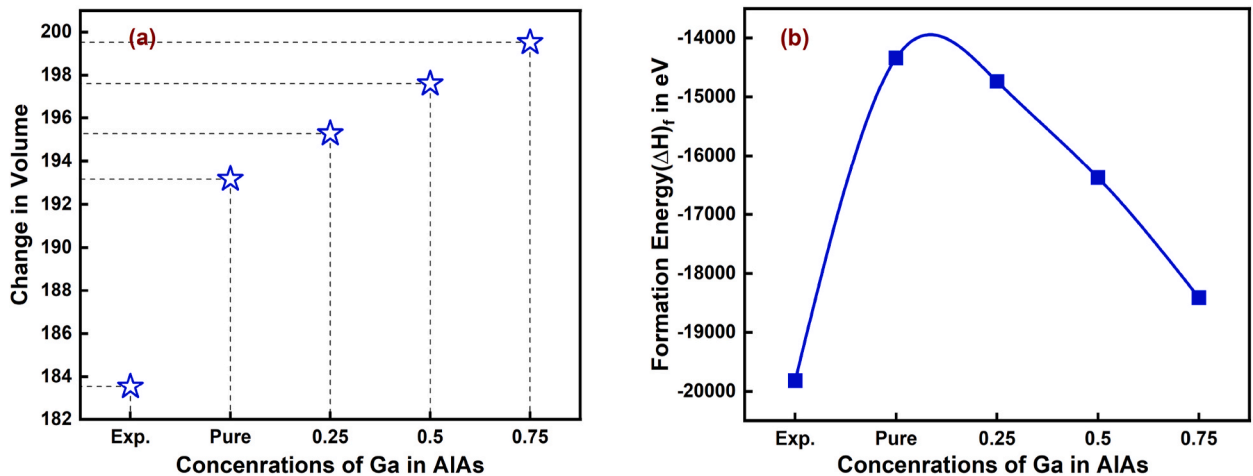


Fig. 2. (a) Change in volume as a function of Ga-concentration doping ( $\text{Al}_{1-x}\text{Ga}_x\text{As}$ : at  $x = 0$  to 0.75) (b) Change in formation energy as a function of Ga-concentration ( $\text{Al}_{1-x}\text{Ga}_x\text{As}$ : at  $x = 0$  to 0.75).

**Table 1**

Geometrically optimized lattice parameters, super cell volume and %age variation in lattice parameters from the experimental values for  $Al_{1-x}Ga_xAs$ : for  $x = 0, 0.25, 0.50, 0.75$

Material	Lattice Parameters (Å)				%age Variation in Lattice Parameters		
	a	b	c	Volume (Å <sup>3</sup> )	a	b	c
Experimental Result (Pure) [29]	5.6611	5.66211	5.6611	183.5330			
Theoretical Result (Pure) [30]	5.6683	5.6712	5.6750	192.4243	2.35	2.61	2.62
Calculated Result (Pure)	5.7806	5.7806	5.7806	193.1652	2.06	2.04	2.06
Calculated Result (25 %)	5.8015	5.8015	5.8015	195.2732	2.04	2.04	2.04
Calculated Result (50 %)	5.8267	5.804	5.8267	197.6084	2.08	2.04	2.08
Calculated Result (75 %)	5.8417	5.8417	5.8464	199.5157	3.0	3.0	3.10

**Table 2**

Geometrically optimized crystal angles and formation energy of  $Al_{1-x}Ga_xAs$  for  $x = 0, 0.25, 0.50, 0.75$

Material	Crystal Angles			Formation Energy ( $\Delta H_f$ ) in eV
	$\alpha$	$\beta$	$\gamma$	
Experimental Result (Pure)	90°	90°	90°	-19821.90
Calculated Result (Pure)	90°	90°	90°	-14336.29
Calculated Result (25 %)	90°	89.99°	90°	-14336.36
Calculated Result (50 %)	89.99°	90°	89.99°	-16373.33
Calculated Result (75 %)	90°	89.99°	89.99°	-18410.60

formation about the interatomic potential, stiffness and structural properties of the material [31]. Elastic constants are obtained as a function of lattice strain by Taylor expansion of the total energy. Elastic constants  $C_{ij}$ , bulk modulus  $B$ , shear modulus  $G$ , Young modulus  $E$ , the anisotropic factor  $A$  and Poisson's ratio  $\nu$  for  $Al_{1-x}Ga_xAs$  have been computed and calculated. To calculate the elastic constants of zinc blende (cubic close packing) structure of  $Al_{1-x}Ga_xAs$ , three elastic parameters, i-e  $C_{11}$ ,  $C_{12}$  and  $C_{44}$  are required [32]. The expression which leads to achieve the elastic constants are;

$$C_{ijk} = \frac{\partial \sigma_{ij}}{\partial \epsilon_{ikl}} = \frac{1}{V} \frac{\partial^2}{\partial \epsilon_{kl} \partial \epsilon_{ij}} \quad (6)$$

Conditions of Born stability:  $C_{11} + 2C_{12} > 0$ ,  $C_{11} - C_{12} > 0$ ,  $C_{11} > 0$ ,  $C_{44} > 0$

$$\text{Bulk modulus : } B = \frac{1}{3} (C_{11} + 2C_{12}) \quad (7)$$

$$\text{Young modulus : } Y = \frac{9BG}{(3B + G)} \quad (8)$$

Shear modulus 'G' is obtained by taking average of 'sheer modulus by Voigt's values' and 'sheer modulus by Reuss values'

$$\text{Sheer modulus : } G_v = \frac{1}{5} (C_{11} - C_{12} - 3C_{44}) \quad (9)$$

$$G = \frac{1}{2} (G_v + G_R) \quad (10)$$

$$\text{Poisson's ratio : } \sigma = \frac{(3B - 2G)}{2(3B + G)} \quad (11)$$

Anisotropic factor (A) is computed and calculated by using the relation [37];

$$A = \frac{C_{44}}{C_{11} C_{12}} \quad (12)$$

Born's Stability criteria:

For pristine AlAs,

$$C_{11} + 2C_{12} = 230.45 > 0, C_{11} - C_{12} = 52.7 > 0, C_{11} = 111.95 > 0, C_{44} = 66.53 > 0$$

For  $Al_{0.75}Ga_{0.25}As$

$$C_{11} + 2C_{12} = 231.85 > 0, C_{11} - C_{12} = 51.1 > 0, C_{11} = 97.35 > 0, C_{44} = 65.86 > 0$$

For  $Al_{0.50}Ga_{0.50}As$ ,

$$C_{11} + 2C_{12} = 169.95 > 0, C_{11} - C_{12} = 52.71 > 0, C_{11} = 91.79 > 0, C_{44} = 59.69 > 0$$

For  $\text{Al}_{0.25}\text{Ga}_{0.75}\text{As}$ ,

$$C_{11} + 2C_{12} = 183.53 > 0, C_{11} - C_{12} = 57.86 > 0, C_{11} = 99.75 > 0, C_{44} = 59.23 > 0$$

Explicitly and implicitly the mechanical properties of the material were calculated using three independent elastic tensors;  $C_{11}$ ,  $C_{12}$  and  $C_{44}$ . Table 3 represents the calculated values. As above, Born criteria justify the mechanical stability of the  $\text{Al}_{1-x}\text{Ga}_x\text{As}$  structure as well as another condition of  $C_{12} < B < C_{11}$ . Hence, all of these are elastically anisotropic. Confirmed by the relation  $2C_{44} = C_{11} - C_{12}$  [33]. Material offers longitudinal resistance satisfied by  $C_{11} > C_{12} > C_{44}$  more than the shape deformation. Degree of resistance to the applied stress is indicated by Young modulus (E) offered by the material against the longitudinal tension [34]. Increasing values of E in the table shows smaller thermal resistance. The brittle character of the material is confirmed by the Pugh's ratio  $B/G < 1.75$  for all structures having values 1.67, 1.40, 1.26, 1.36 for Ga concentrations  $x = 0, 0.25, 0.50, 0.75$  respectively [35]. Material offers larger value of shear moduli G which shows larger tensional sustainability. Mechanical instability is observed when  $C_{44}$  and  $B/C_{44}$  are negative. In Table 4, all values of Poisson ratio ( $\nu$ ) for  $\text{Al}_{1-x}\text{Ga}_x\text{As}$  are less than the borderline of 0.26 to be called a material as brittle [36]. Therefore, mechanically our material is quite suitable for industrial application as a dedicated material like, LEDs, transistors, ICs, LASER diodes, frequency dependent sensors.

### 4.3. Electronic properties

The equilibrium lattice constants obtained are used with the GGA-PBESol scheme to compute the electronic band structures of the binary-intrinsic AlAs and ternary-extrinsic  $\text{Al}_{1-x}\text{Ga}_x\text{As}$ : at  $x = 0$  to 0.75 material with up-rated symmetry lines in the Brillion Zone (BZ). Mechanism of the changed energy bandwidth of the material is explored in this section. Clear insight for the electronic properties, was unraveled by decomposing each band into contributions of s, p and d. The effect of Ga doping on pure AlAs material is observed through the valence band (VB) and conduction bands (CB). Supported by the optimized structures, graphs of the electronic bands are shown in Fig. 3. Fermi-level is close to the CB which shows the n-type character of the AlAs [37]. VB-maxima and CB-minima occur closer to the gamma points in the BZ. By the introduction of trivalent impurity Ga provides holes in the lattice that shifts the material with a p-type character. Fermi level is between the acceptor energy level and valence band and it is close to the valence band then conduction band [38]. The computed band gap value of pure AlAs achieved from GGA PBESol function was 1.478eV. The band gap of AlAs is underestimated compared with the previously reported value of the band gaps. The proficiency of an indirect band gap is smaller than the direct band gap nature [39].

The dedicated results before and after doping of Ga in AlAs of electronic band structure are plotted in Fig. 3 (a - d), and bandgap trend is shown in Fig. 1 (e). It is pictured that MVB and MCB are located at the different points. The behavior is indirect. Fig. 3(b) computed band gap of 1.478eV reduces to 1.012 eV (for  $\text{Al}_{0.75}\text{Ga}_{0.25}\text{As}$ ). Fig. 3(c) calculated band gap of  $\text{Al}_{0.50}\text{Ga}_{0.50}\text{As}$  reduces from 1.012 eV to 0.653eV (for  $\text{Al}_{0.50}\text{Ga}_{0.50}\text{As}$ ). In Fig. 3(d) the band gap of  $\text{Al}_{0.75}\text{Ga}_{0.25}\text{As}$  reduces from 0.653eV to 0.280 eV. The main involvement of overlapping orbital takes place between the  $\text{Al-}3s^2, 3p^1$ , to a converged energy value of  $-107.1299$  eV,  $\text{As-}3d^{10} 4s^2 4p^3$  to a converged energy value of  $-2957.1936$  eV and  $\text{Ga-}3d^{10} 4s^2 4p^1$  which converges to a total energy of  $-2144.9499$  eV. The Band gap values have drastically reduced by the addition of gallium concentrations. For 25 % addition of Ga at the site of Al results in a new smaller gap value of 1.012eV, it is 0.653eV with 50 % addition of Ga and 0.280eV for 75 % of Ga. This energy shift is for the off-center displacement of ions [40]. Trapping of electrons at the Ga doping site causes a defect state inside the  $\text{Al}_{1-x}\text{Ga}_x\text{As}$  accordingly a hole at the Al site shows a rich photo-sensitive feature comprising an additional recombination channel inside the doped material. An exchange role of transfer excitation from the host AlAs to excited Ga is suggested which consists of an additional path for the recombination of photo-generated carriers [41]. It is evident from the results displayed above in graphs, the Fermi-level of doped material modifies more into the valence band. Reduction of the band gap is reasoned by the incorporation of Ga in AlAs. Generally, creates allowed shallow electronic states in the band gap. These states have small ionization energy with the high density of Ga doping, hence these impurity states generate a band. The newly formed band is close to CB or VB edge; henceforth electronic band gap decreases. The computed value of the band gap is much smaller than the reported value in the case of Ga but the core difference does not affect the measurement of the other significant constraints.

We analyze the p-orbitals of Ga become intense in the valence band but the peaks of the structure were found to shift up. Mullikins charges are one of the simplest method for estimating the atomic charges inside the atom. The computed value of Mullikan charge and bond length of pure AlAs is shown in Table 4.

Numerically, effective valence is assessed from a formal charge.

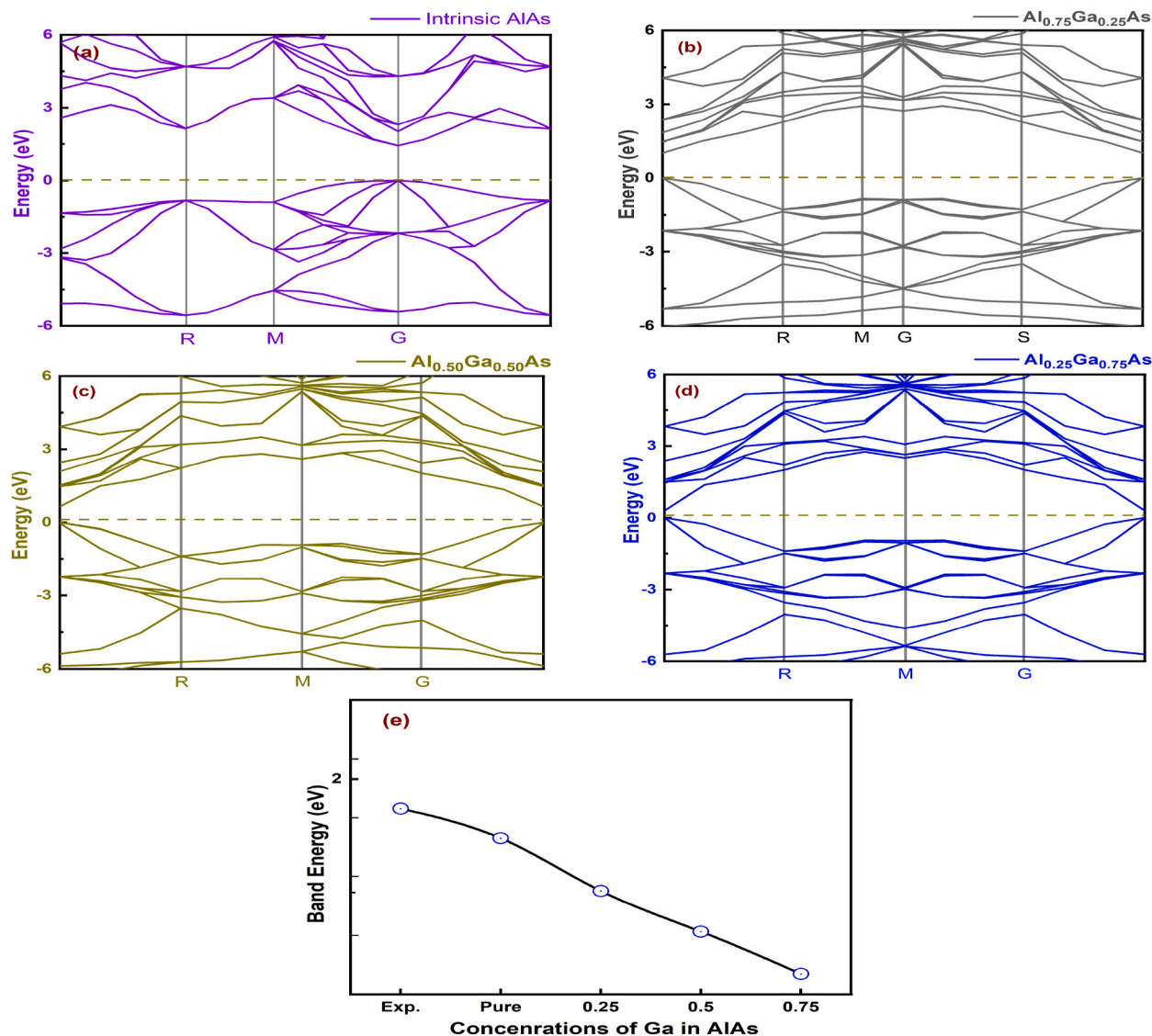
**Table 3**

Reported and Calculated elastic constants  $C_{ij}$  (in GPa), bulk modulus (B) and shear modulus (G), G/B, Poisson's ratio ( $\nu$ ), Young modulus(Y), hardness ( $H_v$ ) and machinability index  $\mu_M$ .

Compound	$C_{11}$ (GPa)	$C_{12}$ (GPa)	$C_{44}$ (GPa)	B(GPa)	G(GPa)	B/G	$\nu$	Y(GPa)	$H_v$	$\mu_M = B/C_{44}$
Reported [7]	101.3	48.4	48.4	66.07	38.0	1.74	0.26	95.67	5.79	1.36
Present work (AlAs)	111.9	59.2	66.53	76.85	45.89	1.67	0.25	114.82	7.65	1.15
$\text{Al}_{0.75}\text{Ga}_{0.25}\text{As}$	97.33	46.2	65.83	63.31	45.16	1.40	0.21	106.45	8.50	1.46
$\text{Al}_{0.50}\text{Ga}_{0.50}\text{As}$	91.79	39.0	59.69	57.37	45.57	1.26	0.18	108.09	9.77	0.96
$\text{Al}_{0.25}\text{Ga}_{0.75}\text{As}$	99.75	41.8	59.23	60.45	44.33	1.36	0.20	106.88	8.91	1.02

**Table 4**Table of values of bandgaps for pure AIAs,  $\text{Al}_{0.75}\text{Ga}_{0.25}\text{As}$ ,  $\text{Al}_{0.50}\text{Ga}_{0.50}\text{As}$  and  $\text{Al}_{0.25}\text{Ga}_{0.75}\text{As}$ .

Material	Band gap (eV)			
	Al	Ga	As	Band gap (eV)
Experimental Result (Pure) [42]	$3s^2 3p^1$	–	$3d^{10} 4s^2 4p^3$	2.24
AIAs (Pure)	$3s^2, 3p^1$	–	$3d^{10} 4s^2 4p^3$	1.478
$\text{Al}_{0.75}\text{Ga}_{0.25}\text{As}$ , (25 %)	$3s^2, 3p^1$	$3d^{10} 4s^2 4p^1$	$3d^{10} 4s^2 4p^3$	1.012
$\text{Al}_{0.5}\text{Ga}_{0.5}\text{As}$ (50 %)	$3s^2, 3p^1$	$3d^{10} 4s^2 4p^1$	$3d^{10} 4s^2 4p^3$	0.653
$\text{Al}_{0.25}\text{Ga}_{0.75}\text{As}$ (75 %)	$3s^2, 3p^1$	$3d^{10} 4s^2 4p_1$	$3d^{10} 4s^2 4p^3$	0.280

**Fig. 3.** Electronic Band Structure of: (a) pure AIAs (b)  $\text{Al}_{0.75}\text{Ga}_{0.25}\text{As}$  (c)  $\text{Al}_{0.50}\text{Ga}_{0.50}\text{As}$  (d)  $\text{Al}_{0.25}\text{Ga}_{0.75}\text{As}$  (e) Trend of decrease in band gap with Ga concentrations (at; x = 0, 0.25, 0.50, 0.75).

Effective valence = abs (Formal charge) – abs (Mulliken charge) [8].

The idea of effective valence is used to understand the distribution of electronic charge inside the molecule and helps in describing its behavior in working state, as shown in Table 5. It can unfold the higher or lower regimes of electron density. After exploring the band gap tuning, we investigate and explain the basis of electronic band structures. To comprehend the electronic reactions of analyzed compounds, we inspected the partial density of state (PDOS), the total partial density of state (TPDOS), the total density of

state (TDOS) and the elemental partial density of state (EPDOS) [43]. p-states are also known as valence band-states and referred to the energy of electron in the VB. VB is the highest occupied band by the electrons at the absolute zero temperature. p-states contributes to form continuous band of allowed energy states for electrons where carriers are loosely bound to the atoms and are mobile as compared to the inner electrons. In this work energy is provided to shift them into the conduction band where they can move freely. d-state also known as ‘conduction band state’ which is the lowest energy band which is partially or empty at the absolute zero. It is worth to note that electrons in CB are the carriers of electrical current in semi-conductors. Hence, these states are highly fundamental in the functioning of semiconductor devices. In this context, graphs of pure and suitably doped Ga are shown in Fig. 4. In Fig. 4(a), PDOS with GGA-PBEsol, for pure AlAs, the maximum peak edge shows the contribution of 3p-state of Aluminum and 3d, 4p-state of Arsenic with energy level of  $-35.0\text{eV}$ – $33.9\text{eV}$  at the peak value 67.8 electrons/eV within the valence band (VB) whereas s and p states are observed with minor contributions of states of both, Al and As within the energy range of  $-10.1\text{eV}$  to  $-1.3\text{eV}$  at the maxima of 7.2 electrons/eV. In case of Ga addition ( $x = 0.25, 0.50, 0.75$ ) as shown in Fig. 4 (b,c,d) respectively, the stronger hybridization of d-states appears near the Fermi-level because of the contribution of more density of states of Ga which causes narrowing the band gap. Stronger the hybridization character, less will be the energy require to move carriers from valence to conduction band. More carriers with less gap energy are highly suitable for the low power materials in the field of electronic appliances [44]. Hence, the graphs of PDOS are comprehensively the compromised signatures of ternary semiconductor ( $\text{Al}_{1-x}\text{Ga}_x\text{As}$ ) for its consistency with reliable experimental path to produce the material in the labs and industry. Fig. 4 (e) is the comparative plot of TPDOS for all concentrations. TPDOS with GGA-PBEsol shows the maximum peak edges shifted from  $-1.28\text{eV}$  to  $0.62\text{eV}$  in VB and maximum contribution in the CB is due to the transition of free electrons from the VB.

The dotted vertical lines in the figures above indicates the Fermi level at the energy value of zero electron volt. The graphs of TPDOS and TDOS are shown in Fig. 4 (e and f) are with intrinsic and Ga-doped concentrations which shows appreciable large area involvement for Ga (3d, 4s and 4p-states) with the maximum strong contribution of 6.07electrons/eV at  $-1.59\text{eV}$  of energy range. For all Ga-concentrations maximum involvement was noted for CB respectively. Fig. 4(f) is the frequent chart of qualitative picture of the electronic structure of the material under study with all concentrations. Edges of the structures were found to shift up to the lower energy range of  $2.1\text{eV}$ – $4.3\text{eV}$ . The overall required peaks are within the energy range of  $1.06\text{eV}$ – $5.88\text{eV}$  at the maximum peak of 5.88 electrons/eV. Comparative to other states, the strong contribution is carried with the combination of p and d states from the third and fourth subshells of the ingredients, especially Ga and As as obvious from fig. (e). The contribution of both (4p-3d) Ga and Al states shifts edges from  $0.62\text{eV}$  to  $5.32\text{eV}$  because of the movement of free electrons [44]. The orbital study of the density of states reveals that VB is mostly found to be constructed by Al-3p and As-4p orbitals while CB is mainly composed of Al-3s, Al-3p and As-4d states. Tailoring the bonding response of pure AlAs and Ga-doped, to provoke the character of the bandgap and also describe the electronic charge shifted and bonding response computed the total density. The charge density represents the strong ionic behavior as can be appreciated along peaks. The creation of allowed shallow states of smaller ionization potential are more friendly towards the creation of smaller interband gaps, here which is obtained by Ga contributions. Partial density of states (PDOS) is justified by the maximum contribution of the orbital [45]. The projected density of states in Fig. 4(e) shows that Ga-4p donates to the top of the valence band, so it is a p-type doping [46]. An unoccupied Ga-4p orbital impurity give the impression in the energy gap below conduction band. Due to the emergence of new energy levels, the minimum energy of electrons from the VB to the CB changes.

The density of the state of elements is directly related to the dispersion relation of properties of the system. It represents several equivalent energy maxima in the VB and the number of equivalent energy minima in the CB. The plot of the elemental partial density of states (EPDOS) in Fig. 5 (a) for intrinsic AlAs is 3s-state of Al is contributing in VB shown with the peak value of 3.0 electrons/eV with the energy edge shift of  $-5.75\text{eV}$  to  $-3.70\text{eV}$ , whereas Aluminium 3p-state in pure AlAs is contributing in the CB with the peak of 5.65 electrons/eV having edge shift energy of  $3.98\text{eV}$ – $5.29\text{eV}$  and Al 3p-state in 0.25Ga-doped are observed with the peak of 3.93 electrons/eV along with edge shift energy of  $3.98\text{eV}$ – $5.68\text{eV}$  which is very close in value to the 3p state edge shift of intrinsic AlAs. The charge density represents a strong ionic behavior as can be seen along Ga–Al bond and Ga–As bond indicates has a strong covalent nature. In Fig. 5(b) PDOS plot for Arsenic shows its orbital contribution in the VB with its 4p-state in the pure AlAs to the peak value of 4.38 electrons/eV with the energy edge shift of  $-2.24\text{eV}$  to  $-1.09\text{eV}$  whereas As 4s-state in pure 0.75Ga is contributing in the CB with the peak of 5.34 electrons/eV having edge shift energy of  $2.11\text{eV}$ – $3.26\text{eV}$ . Another prominent peak of As is at 5.57 electrons/eV 0.50Ga-doped are observed with edge shift energy of  $1.01\text{eV}$ – $05.3\text{eV}$  showing the 4s-state contribution in the CB. Similarly, the results of EPDOS for Ga orbitals are studied by Fig. 5(c). Peak in VB is due to the involvement of 4s orbital with the 0.75Ga-doped with the maximum of 4.28 electrons/eV showing the energy shift of  $-4.96\text{eV}$  to  $-2.78\text{eV}$ . 4p-state of Ga contributes in the CB at the peak of 3.69 electrons/eV having shift of  $0.56\text{eV}$ – $3.7\text{eV}$  and finally a 3.23 electrons/eV peak is studied with net shift of  $1.34\text{eV}$ . Evident contribution of EPDOS is due to 3s and 3p-states for Al and 3d, 4s and 4p-states for As and Ga [47]. This detailed analysis elaborates the contribution of states which are responsible for the availability of carriers for determining the carrier concentration and energy distribution of carriers within the  $\text{Al}_{1-x}\text{Ga}_x\text{As}$  semiconductor which are the gross roots for the reduction of band gap.

**Table 5**

The calculated value of Mulliken charge and bond Lengths of AlAs with GGA.

Species	S	p	d	Charge	Bonds	Population	Length	Reported Length	Effective Valence
Al	1.10	1.60	0.00	1.44	Al–As	0.65	2.50	2.49	0.30
As	1.43	3.83	10.00	10.00	Al–As	0.65	2.50	2.49	0.26

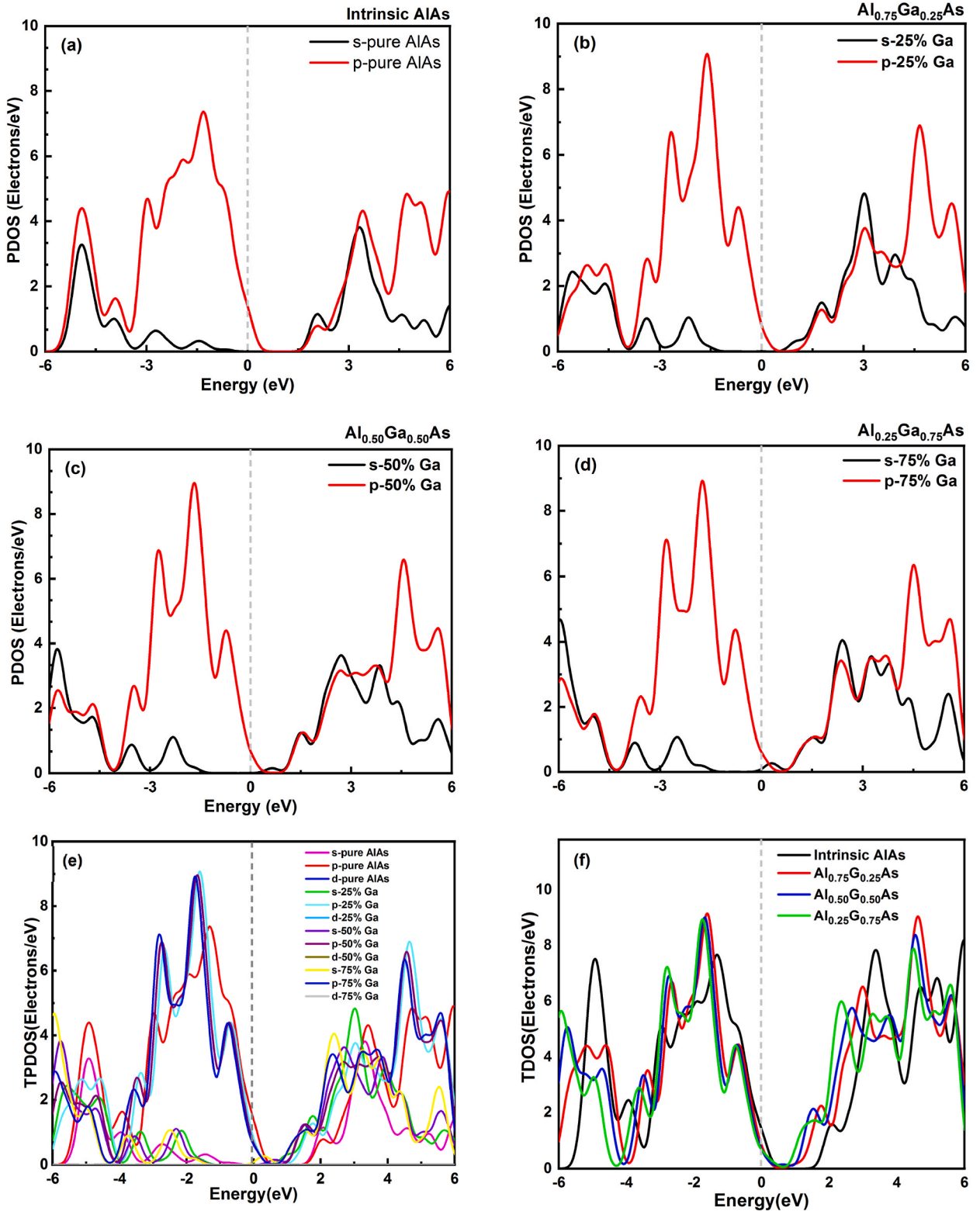


Fig. 4. Partial density of states (PDOS) of: (a) pure AlAs (b)  $\text{Al}_{0.75}\text{Ga}_{0.25}\text{As}$  (c)  $\text{Al}_{0.5}\text{Ga}_{0.5}\text{As}$  (d)  $\text{Al}_{0.25}\text{Ga}_{0.75}\text{As}$  (e) total PDOS and (f) TDOS.

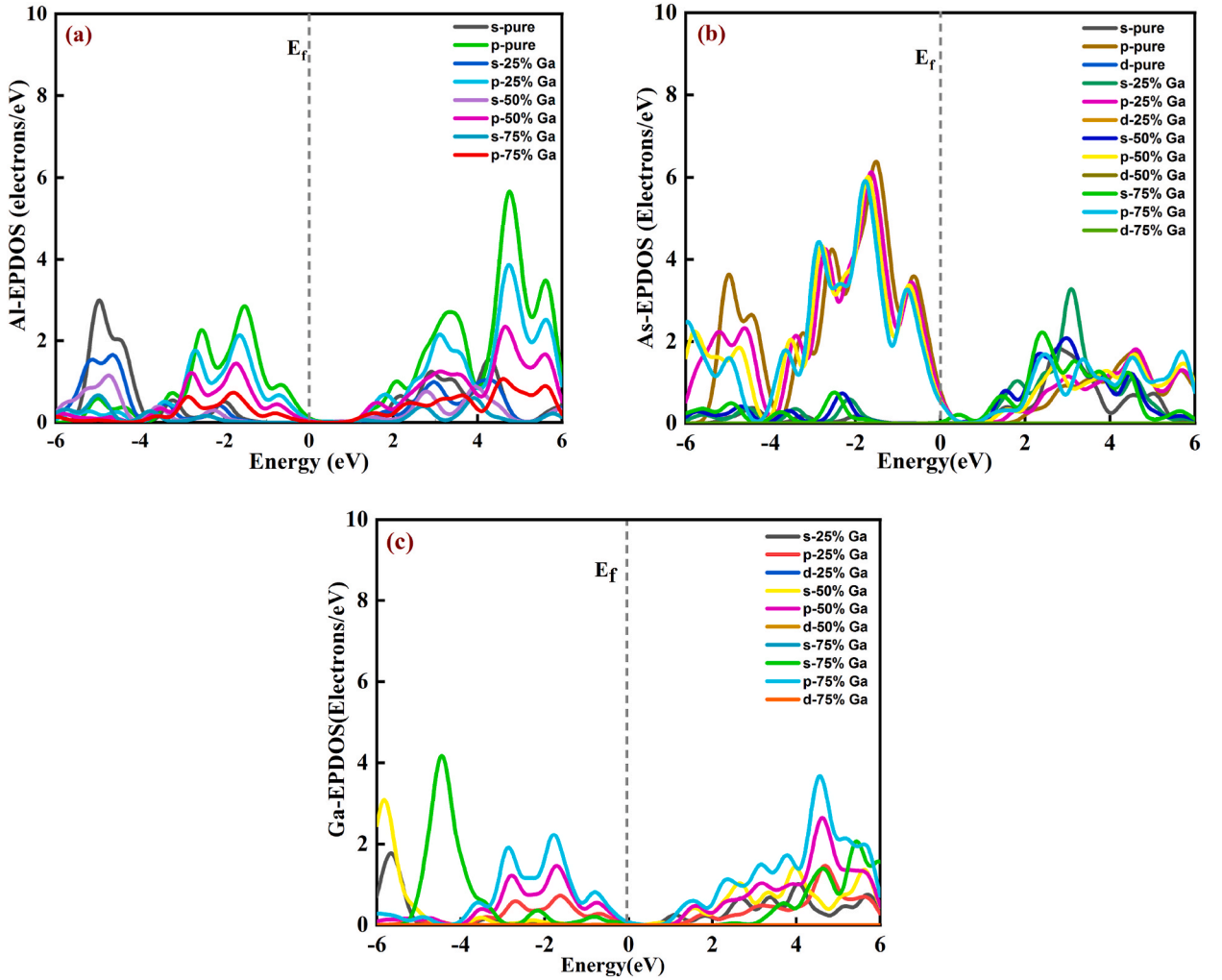


Fig. 5. Elemental partial density of states (EPDOS) of: (a) Al (b) As and (c) Ga.

#### 4.4. Theory and results of optical properties

##### 4.4.1. Dielectric function

Understanding the dielectric function of a material is vital in various fields including optics, photonics, material science and device engineering. In optics, dielectric function relates how a material interacts with the electromagnetic radiations such as light. It also characterizes response of the material to an applied electric field or electromagnetic wave. The research on the optical response of a material is crucially important to show the promising investigation of the material for optoelectronic applications. The apparent interface among the atoms and incident photons is designated by a complex dielectric function that depends upon its frequency. Complex DF is predominantly tried for electronic structure modification and can be used to comprehend the optical response. A real part of the dielectric function characterizes the energy stored inside the medium while the imaginary part relates to the absorption behavior in the electronic band structure of the material [48]. These parameters can be appreciated by the knowledge of complex dielectric functions comprising of two parts, real and imaginary;

$$\varepsilon(\omega) = \varepsilon_1(\omega) + i\varepsilon_2(\omega) \quad (13)$$

Real part  $\varepsilon_1(\omega)$  and imaginary  $i\varepsilon_2(\omega)$  of the dielectric function  $\varepsilon(\omega)$  are handled by the perturbation theory. The frequency-dependent real part of the dielectric function can be resulting from the Kramers-Kronig relation [49].

$$\varepsilon_1(\omega) = 1 + \frac{2}{\pi} P \int_0^{\infty} \frac{\omega' \varepsilon_2(\omega')}{\omega'^2 - \omega^2} d\omega' \quad (14)$$

here,  $P$  represents the principal value of the integral. And imaginary part is given by;

$$\varepsilon_2(\omega) = \left( \frac{4\pi^2 e^2}{m^2 \omega^2} \right) \sum_{ij} \int \langle i | M_{ij} | j \rangle^2 f_i (1 - f_j) \delta(E_j - E_i - \omega) d^3 k \quad (15)$$

Photon energy is desired for all-optical reactions. Using the above optical parameters  $\varepsilon_1(\omega) + i\varepsilon_2(\omega)$ , the frequency-dependent reflectivity,  $R(\omega)$  can be computed by using the following equations:

$$R(\omega) = \frac{|\sqrt{\varepsilon(\omega)} - 1|^2}{\sqrt{\varepsilon(\omega)} + 1} \quad (16)$$

The absorption coefficient is given by Beer's law

$$\alpha = \frac{2k\omega}{c} = \frac{4\pi k}{c} \quad (17)$$

The followings are the deliberated equations referred to the frequency-dependent optical constants;

$$\text{Extinction coefficient : } K(\omega) = \left[ \frac{1}{\sqrt{2}} \left\{ (\varepsilon_1(\omega)^2 + \varepsilon_2(\omega)^2)^{\frac{1}{2}} - \varepsilon_1(\omega) \right\}^{\frac{1}{2}} \right] \quad (18)$$

$$\text{Energy loss : } L(\omega) = \text{Im}[-1/\varepsilon_1(\omega)] \quad (19)$$

Where,  $n$ ,  $L$ ,  $K$ , and  $r$  represent the refractive index, loss function, extinction coefficient, and reflectivity respectively. Optical properties are computed and explored for the ZB structure of pristine and Gallium doped Aluminium Arsenide by GGA-PBESol. For reliable calculation of the optical properties especially for optoelectronic devices, the study of both the optical and electronic band gap play a fundamental role in the design of optoelectronic devices [50]. Therefore, it is very important to enhance the number of  $k$ -points in the involved Brillouin one for electron as well as phonon-assisted transitions. Keeping this point in view, 1000  $k$ -points were set [51].

The determined dielectric functions are represented in Fig. 6 (a and b). These graphs represents the optical spectra of the real and imaginary part for pure and Ga-doped AlAs ternary semiconductor. Real part in Fig. 6 (a) starts at a non-zero value and continues to smash a maximum intensity at 20.3 peak shown for 0.75Ga for the photon energy value of 1.2eV. This elaborates successful contribution of 0.75Ga concentration as storage of optical energy by the  $\text{Al}_{0.25}\text{Ga}_{0.75}\text{As}$ . The 4s and 4p-states of Ga hybridized with 4 h states orbital of Arsenic shows their contribution to the transfer of photon energy to the electrons of these states [52]. In case of 0.50Ga inclusion, the maximum peak is noted at 18.3 at the 1.5eV of energy which also favors the contribution of Gallium in AlAs in the IR and visible range of incident light like as 0.75Ga. The 0.25Ga peak is 16.8 for the photon energy of 1.86eV whereas for pure its value is 17.16 at 2.62eV shows the less absorption coefficient in the Lambert Beers law. These results concludes the astonishing scaffold of the doped ternary semiconductor for its application in the field where significant role of polarization of material is required [53]. When frequency of light falling on the material gradually increases, the optical gain of the computed material showed increased response as peaks are shifted from lower to higher values showing conversion of more energy into use by the device.

Similarly, the results of the imaginary part of dielectric function is shown in Fig. 6 (b). The peaks from maximum to minimum are; 21.4, 21.1, 20.2 and 19.8 for AlAs,  $\text{Al}_{0.25}\text{Ga}_{0.75}\text{As}$ ,  $\text{Al}_{0.50}\text{Ga}_{0.50}\text{As}$  and  $\text{Al}_{0.75}\text{Ga}_{0.25}\text{As}$  respectively. And corresponding energy values are 4.0eV, 3.8eV, 3.6eV and 3.9eV. The peaks shifts to lower values from 21.4 to 19.8 by the addition of Ga in the pristine AlAs at zero pressure, is insistent with the changed computed values in the optical band gaps as discussed above in the band calculation shows linear absorption response [54]. These values illustrates the optical power loss of the material due to the interband transitions. It is evident from the optical response that materials that are applicable in different optoelectronic systems are extensively used and

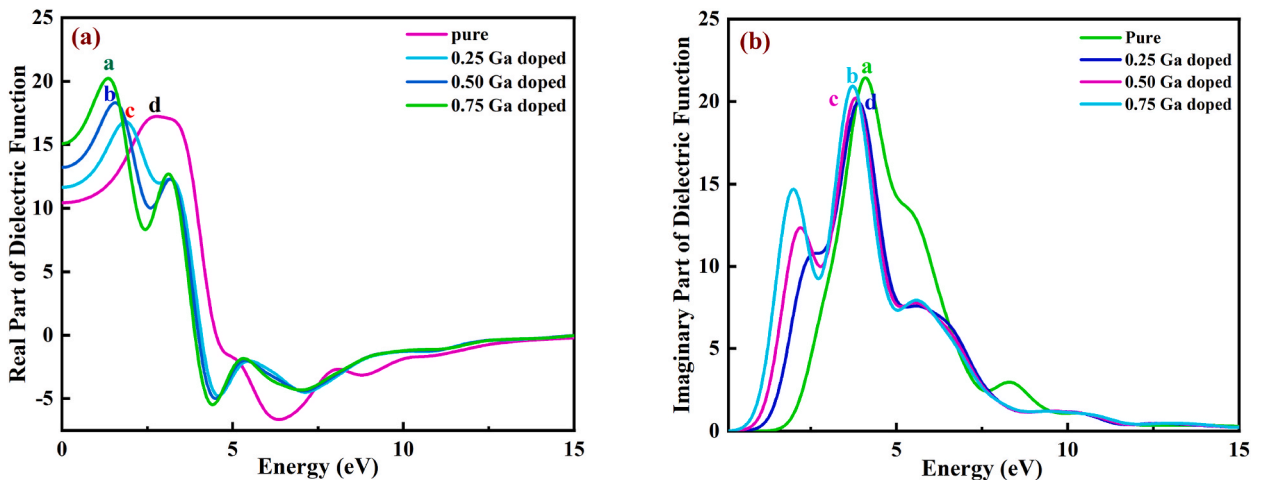


Fig. 6. Dielectric function of  $\text{Al}_{1-x}\text{Ga}_x\text{As}$  for ( $x = 0, 0.25, 0.50$  and  $0.75$ ) by GGA-PBESol: (a) Real part (b) Imaginary part.

interpreted by the calculation of dielectric function. Hence, optoelectronic devices heavily depends upon such behavior of the semiconductors material. Therefore, these compositions are quite suitable for solar cells and detectors [55].

#### 4.4.2. Refractive index

One of the interaction between light and matter is refractive index which causes light to change its path and speed within the material [56]. Bending and changing speed of light is the function of wavelength of light passing through it. The propagation depth of light in the material depends upon its refractive index. Lesser refractive index indicates more transmission. Equation for refractive index:

$$n(\omega) = \left[ \frac{1}{\sqrt{2}} \left\{ (\epsilon_1(\omega)^2 + \epsilon_2(\omega)^2)^{\frac{1}{2}} + \epsilon_1(\omega) \right\}^{\frac{1}{2}} \right] \quad (20)$$

This phenomenon start just at the interface as light inters through it. Materials with higher refractive indices tends to bend the light more which makes them useful for lenses and optical devices. This also links to other important optical properties, like as reflectivity, transmittance and dispersion [57]. There are two parts of refractive index; real and imaginary. Real part ( $n$ ) describes the speed of light in the material whereas imaginary part is the extinction co-efficient ( $k$ ) which is the measure of how light is absorbed at a given wavelength.

$$n(\omega) = n(\omega) + ik(\omega) \quad (21)$$

Both the parts  $n$  and  $k$  are wavelength dependent so vary over the electromagnetic wave spectrum. Refractive index of intrinsic AlAs and with incorporations of Ga (at;  $x = 0, 0.25, 0.50, 0.75$ ) are elaborated in Fig. 7 (a,b), obtained by GGA-PBEsol. From Fig. 7 (a) the real parts  $n$  is the normal refractive index at zero frequency having indices 3.2, 3.4, 3.6 and 3.8 for pure AlAs,  $\text{Al}_{0.75}\text{Ga}_{0.25}\text{As}$ ,  $\text{Al}_{0.50}\text{Ga}_{0.50}\text{As}$  and  $\text{Al}_{0.25}\text{Ga}_{0.75}\text{As}$  respectively. These values of  $n$  increases regularly with the incorporation of Ga concentrations. The band gap is inversely related to the refractive index at zero frequency. The maximum noted values of indices are 4.4 (for pure), 4.1 (for  $\text{Al}_{0.75}\text{Ga}_{0.25}\text{As}$ ), 4.3 (for  $\text{Al}_{0.50}\text{Ga}_{0.50}\text{As}$ ) and 4.5 (for  $\text{Al}_{0.25}\text{Ga}_{0.75}\text{As}$ ) observed for the photon energies of 3.5 eV, 1.9eV, 1.6 eV and 1.4eV respectively. These result concludes that as addition of Ga increases there is decrease in refractive index for 0.25Ga and 0.50Ga. This trend clarify the propagation strength of the material suitable for the 0.25Ga and 0.50Ga for the photon of energy from 1.6eV to 1.8eV. This is obtained by producing the thin films, optical lenses and pigments.

Imaginary parts in Fig. 7 (b) called extinction coefficient  $k$  is directly related to absorption coefficient of the material. The main four peaks of extinction co-efficient are 3.2, 4.2, 4.1 and 3.2 for Ga incorporation ( $x = 0.75, 0.50, 0.25$  and 0). As the real and imaginary parts of refractive index are inversely to each other. Therefore, to cut the whole story short it can straight forwardly be said that energy range for which the material is not good for propagation of light, it will be useful for the absorption purpose. This deals with the nature of allowed and un-allowed transitions and the real part is the indication of degree of polarization [58]. The gradual change in the bandgap of  $\text{Al}_{1-x}\text{Ga}_x\text{As}$  offers talented results for optoelectronic devices. It shelters a full spectrum of wavelengths from visible to UV. This deals with the nature of allowed and un-allowed transitions and real part is the indication of degree of polarization. The profile of these values suggests absorbance in terms of energy range from 3eV to 7.8 eV, which certifies the competency of ternary semiconductor material as a good absorber rather than intrinsic AlAs, likewise a good candidate for optoelectronic especially for solar cell applications [59].

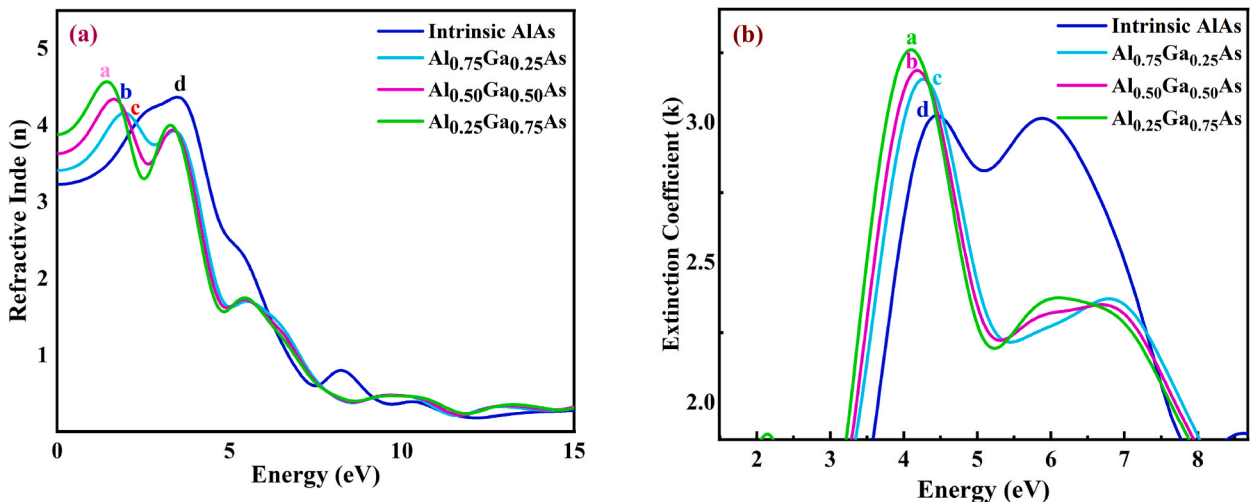


Fig. 7. (a) Refractive Index ( $n$ -real) and (b) Refractive Index ( $k$ -extinction coefficient); of pure AlAs and ternary semiconductor  $\text{Al}_{0.75}\text{Ga}_{0.25}\text{As}$ ,  $\text{Al}_{0.5}\text{Ga}_{0.5}\text{As}$  and  $\text{Al}_{0.25}\text{Ga}_{0.75}\text{As}$ .

#### 4.4.3. Reflectivity and absorption

One of the very basic optical phenomenon is reflection of light that is the bouncing back of light from the surface of the material. Infect electrons of the material that absorbs energy when come in contact with the light. Later they release energy back in the form of light [60]. This replicated back part of the light is liable for the shiny, lustrous appearance of metals. Best material surfaces for reflecting of light are of glass mirrors and polished metals, although all surfaces will reflect light to some extent [61]. This phenomenon is very similar to the heat a material. Heat is assisted by phonon assisted transition called thermalization whereas reflection is assisted by photon assisted transition. Thin surfaces of many materials become good conductors of light so their study is very impressive [62]. It is important to realize that sum of reflection (R), transmission (T) and absorption (A) is always equal to one i-e  $R + T + A = 1$

$$\text{Reflectivity in terms of } n \text{ and } k : r(\omega) = \frac{\{(n-1)^2 + K^2\}}{\{(n+1)^2 + K^2\}} \quad (22)$$

The reflectivity and absorptions of pristine AlAs and doped AlAs are shown in Fig. 8 (a, c) with their trends in Fig. 8 (b, d) respectively. The prominent peaks for each combination; binary and ternary semiconductor are shown in Fig. 8 (a) 0.69, 0.67, 0.66 and 0.64 are maximum peak for AlAs,  $\text{Al}_{0.75}\text{Ga}_{0.25}\text{As}$ ,  $\text{Al}_{0.50}\text{Ga}_{0.50}\text{As}$  and  $\text{Al}_{0.25}\text{Ga}_{0.75}\text{As}$  respectively. These values of R decreases regularly with the incorporation of Ga. We see reflectivity is inversely related to the increasing amount of Ga. The maximum noted values of reflectivity are observed for the photon energies of 11.9eV, 8.17eV, 8.1eV and 8.0eV respectively. The reflectivity is directly with the band gap. Lower band gap (0.28eV) of  $\text{Al}_{0.25}\text{Ga}_{0.75}\text{As}$  shows smallest strength of reflectivity in Fig. 8(a). The lower energy values of the all concentrations have more throughput than the pristine AlAs. This trend clarify the gradual propagation strength of the material assisted by Ga suitable for the optical sensors and LEDs.

To quantify the optical absorption in relations of optical density (O.D), which is also called as the absorbance, we use;

$$O.D = -\log_{10}\left(\frac{I(l)}{I_0}\right) \quad (23)$$

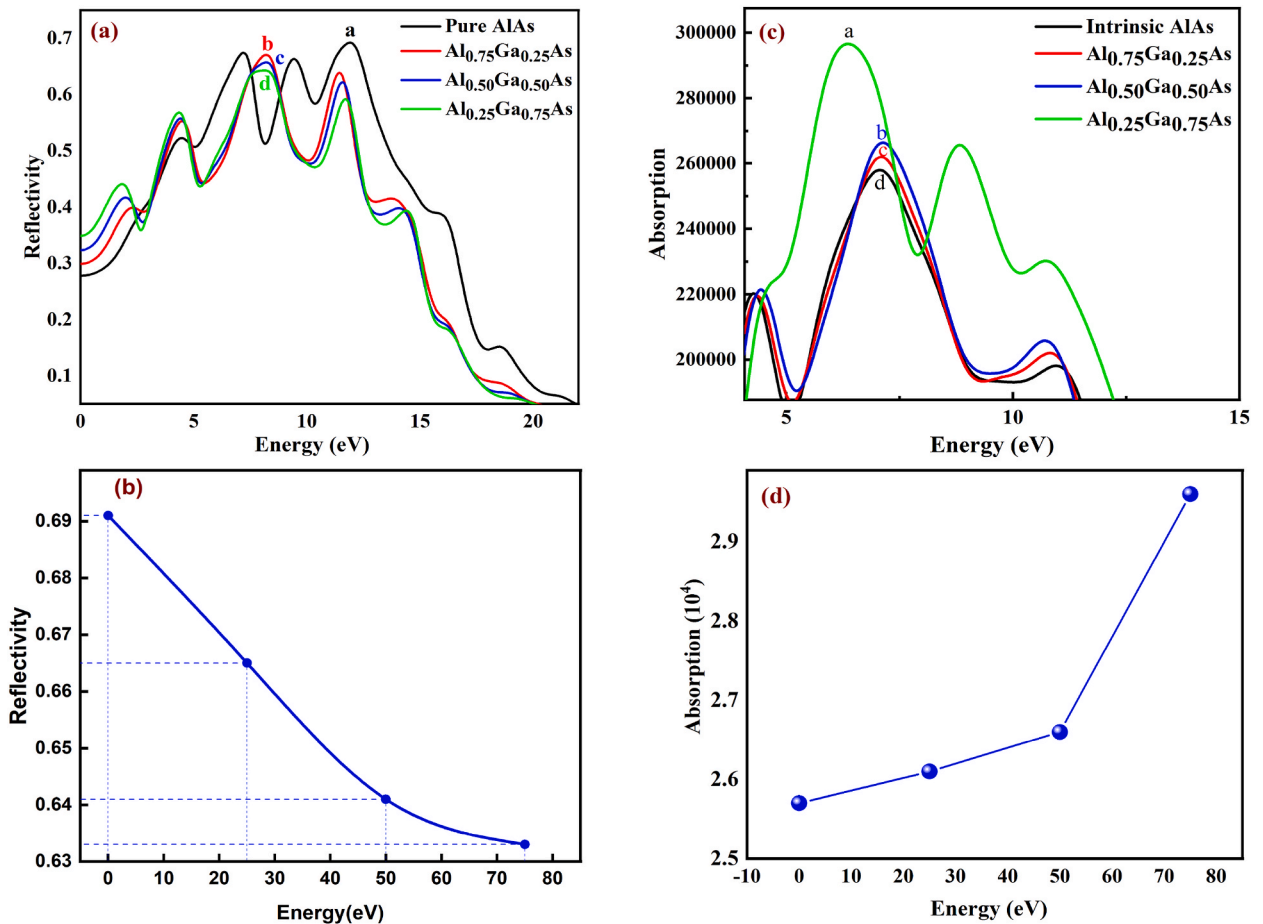


Fig. 8. (a, b) Reflectivity and trend of change in Rreflectivity of  $\text{Al}_{1-x}\text{Ga}_x\text{As}$  for  $x = 0, 0.25, 0.50, 0.75$  by GGA PBEsol (c, b) Absorption and trend of change in Absorption of  $\text{Al}_{1-x}\text{Ga}_x\text{As}$  for ( $x = 0, 0.25, 0.50, 0.75$ ) by GGA-PBEsol.

The term  $l$  is the length of the absorbing medium. The O. D is directly related to the absorption coefficient  $\alpha$  by Ref. [63];

$$O.D = \frac{\alpha l}{\log_e(10)} = 0.434 \alpha l \quad (24)$$

The study of absorption is more likely to be important than the reflection, a quantum approach to study the inside response of material for incident light. For the absorption phenomenon significant peaks for all concentrations are computed and demonstrated along with their trend by Fig. 8 (c, d) respectively. In Fig. 8 (a) the absorption values are 2.96a.u, 2.66a.u, 2.62a.u and 2.58a.u with the multiple of  $10^4$  are maximum peak for  $\text{Al}_{0.25}\text{Ga}_{0.75}\text{As}$ ,  $\text{Al}_{0.50}\text{Ga}_{0.50}\text{As}$ ,  $\text{Al}_{0.75}\text{Ga}_{0.25}\text{As}$ , and AlAs by the peaks a, b, c and d respectively. Absorption values are directly with the amount of doping content. The peaks are noted for the photon energies of 6.31eV, 7.11eV, 7.09eV and 7.06eV respectively. Absorption trends in Fig. 8 (d) are inversely with the band gap. The overlapping of higher energy states 3p, 4s and 4d of Ga and As provides higher absorption level for less photon energies as clear from the graph [64]. This trend clarifies the gradual propagation strength of the material assisted by Ga suitable for the optical sensors and LEDs.

#### 4.4.4. Conductivity

Conductivity is absolutely related to the concentration of free charge carriers electrons and holes. Due to the generation of free carrier, conductivity increases after the absorption of photons with inter band transition. It becomes zero with the at high energy limits [65].

The real part of the optical conductivity signifies absorption and the imaginary part represents losses in terms of the induced electric field. Peaks in Fig. 9(a) provide the picture of how real part of the conductivity is suddenly decreased by Ga addition in AlAs. The peak 10.7 of pure AlAs at energy of light 4.7eV reduces to 9.4 by the gradual introduction of Ga for;  $x = 0.25, 0.50$  and  $0.75$  for the light energy of 4eV to the 3.9eV. Hence, prominent change in conductivity is noted along with the brief reduction in light energy. The relation of real part of conductivity is direct with the band gap. The local responsible are the excitons by the inter transitions from VB to the CB [66]. Fig. 9(b) is the evidence of peak reduction of imaginary part of conductivity from 6.5 to 4.6 with is healthy values for reduced loss of optical energy. These obtained values are carried with the increased impact, 6eV–7.2eV of light energy. These computed results are determined for experimental work to produce in the laboratory.

#### 4.4.5. Optical energy loss

Optical losses may comprise of light capable of generated an electron-hole pair. Lesser energy losses means more will be the optical efficiency of the material. The imaginary part of dielectric function describes the loss of light in the form of attenuation. From Fig. 10 in the case of pure AlAs, the loss of incident light energy is highest from 13.3eV to 18.2eV and with the gradual increment of the Ga concentrations due to overlapping of higher orbitals 4s and 4p-states of Ga and As. Peaks of loss reduces significantly from 6 to 4.4 for AlAs to  $\text{Al}_{0.75}\text{Ga}_{0.25}\text{As}$ , respectively. For Ga, the strong peak near 15.02 eV is mainly caused by the bulk plasmon excitation due to the overlapping of higher energy states. Light below the plasma frequency is reflected by the material as electrons monitors the electric field of light [67]. High losses may cause 'return losses' for the steady input supply. The sudden decrease in the loss value is very impressive impact of the Ga as impurity. This remarkable computational work highly appreciates the incorporation of Ga into the AlAs.

## 5. Conclusion

Optimized crystal structure of Aluminium Gallium Arsenide in which gallium as impurity is determined with stable atomic positions and lattice parameters. The accuracy of our calculations is verified by comparing the calculated lattice constants with available

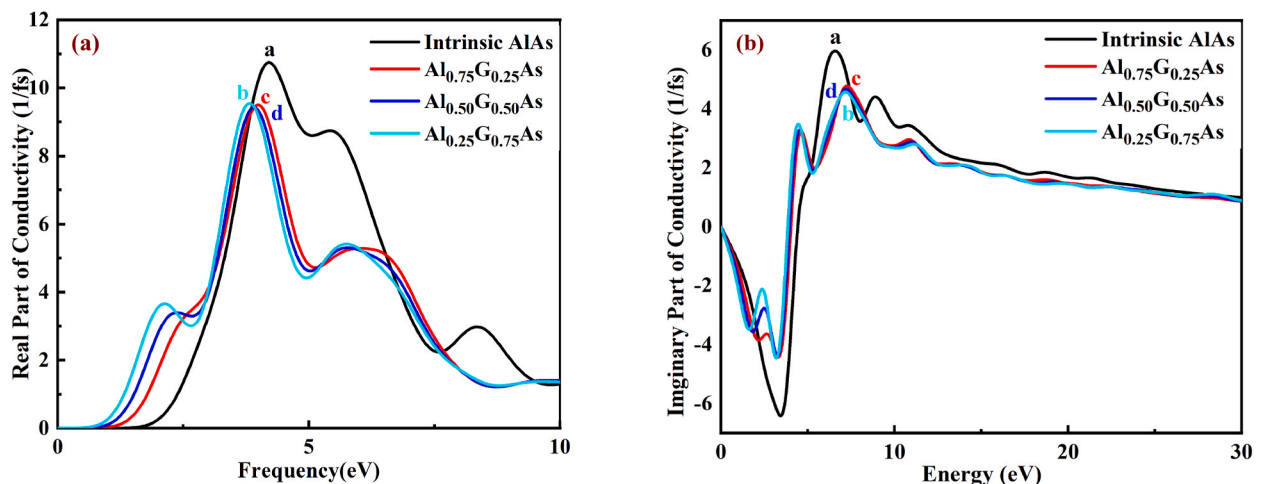
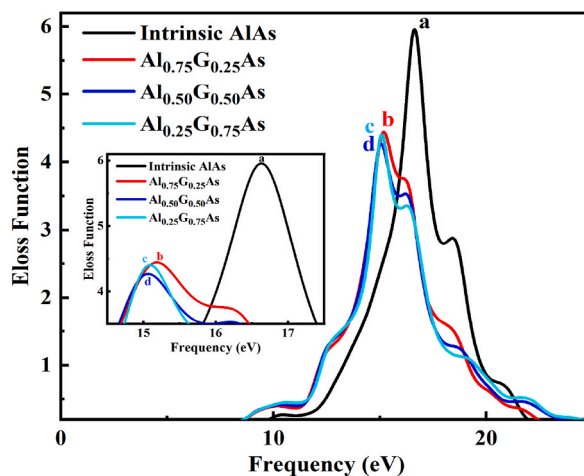


Fig. 9. (a) Real part and (b) Imaginary part: of Conductivity; for pure AlAs and ternary its alloy  $\text{Al}_{0.75}\text{Ga}_{0.25}\text{As}$ ,  $\text{Al}_{0.5}\text{Ga}_{0.5}\text{As}$  and  $\text{Al}_{0.25}\text{Ga}_{0.75}\text{As}$ .



**Fig. 10.** Energy loss as function of frequency of pure AlAs and ternary compound  $\text{Al}_{0.75}\text{Ga}_{0.25}\text{As}$ ,  $\text{Al}_{0.5}\text{Ga}_{0.5}\text{As}$  and  $\text{Al}_{0.25}\text{Ga}_{0.75}\text{As}$ .

experimental data. Different concentrations of Ga as impurity in AlAs caused gradual increment in lattice parameters from 2 % to 2.8 % and hence increased volume of the cell leads to decrease in bandgap from 1.7eV to 0.28eV. The mechanical absorbable are highly excellent tailoring source by adjusting their lattice parameters, electronic orbitals, bonding pattern and crystal structure interatomic distances showed excellent comparison of Bulk modulus (66.07–76.85), Young modulus (95.67–106.88), Sheer modulus (38.0–44.33), hardness (5.79–8.91) and machinability (1.36–1.46) with the reported data. For aluminum gallium arsenide (AlGaAs), the elastic constants can vary depending on the specific composition and crystal structure. The graphs of optical properties crealy trends to the lower value of energy showing their dedication in the low energy devices. Some properties are found to overwhelm much then the theoretical reports for highly improved efficient electronic and optoelectronic applications.

Hence, the dependence of lattice parameters, elastic constants, band gap and optical properties on Ga content in AlAs is of great importance for its use as a determinant material in electronic and optoelectronics devices.

#### CRediT authorship contribution statement

**Anwar Ali:** Writing – original draft. **Abdul Waheed Anwar:** Supervision. **Muhammad Moin:** Writing – review & editing, Writing – original draft, Methodology. **Mehrunisa Babar:** Writing – review & editing. **Udayabhaskararao Thumu:** Formal analysis.

#### Declaration of competing interest

The authors declare the following financial interests/personal relationships which may be considered as potential competing interests: Abdul Waheed Anwar reports a relationship with University of Engineering and Technology, Lahore, Pakistan. That includes: non-financial support. If there are other authors, they declare that they have no known competing financial interests or personal relationships that could have appeared to influence the work reported in this paper.

#### References

- [1] D.A. Neamen, *Semiconductor Physics and Devices*, third ed., Editorial: Mc Graw Hill, 2003.
- [2] S. Adachi, GaAs, AlAs, and  $\text{Al}_x\text{Ga}_{1-x}\text{As}$ : material parameters for use in research and device applications, *J. Appl. Phys.* 58 (3) (1985) R1–R29.
- [3] L. Guo, Structural, energetic, and electronic properties of hydrogenated aluminum arsenide clusters, *J. Nanoparticle Res.* 13 (2011) 2029–2039.
- [4] D.V. Shenai-Khatkhate, et al., Environment, health and safety issues for sources used in MOVPE growth of compound semiconductors, *J. Cryst. Growth* 272 (1–4) (2004) 816–821.
- [5] N. Afzal, M. Devarajan, K. Ibrahim, Effects of indium mole fraction on the physical characteristics of magnetron sputtered  $\text{In}_x\text{Al}_{1-x}\text{N}$  films, *J. Alloys Compd.* 652 (2015) 407–414.
- [6] A. Smith, et al., Cross-sectional scanning tunneling microscopy study of GaAs/AlAs short period superlattices: the influence of growth interrupt on the interfacial structure, *Appl. Phys. Lett.* 66 (4) (1995) 478–480.
- [7] F. Annane, et al., First principle investigation of AlAs and AlP compounds and ordered  $\text{AlAs}_1-x\text{Px}$  alloys, *Comput. Mater. Sci.* 50 (2) (2010) 274–278.
- [8] R. Moussa, et al., Structural, electronic, optical, thermodynamic and elastic properties of the zinc-blende  $\text{Al}_x\text{In}_{1-x}\text{N}$  ternary alloys: a first principles calculations, *J. Phys. Chem. Solid.* 119 (2018) 36–49.
- [9] S. Lany, Semiconducting transition metal oxides, *J. Phys. Condens. Matter* 27 (28) (2015) 283203.
- [10] A. Bentayeb, et al., Structural, electronic, and optical properties of  $\text{AlN}_x\text{Sb}_{1-x}$  alloys through TB-mBJ-PBEsol: DFT study, *J. Comput. Electron.* 18 (3) (2019) 791–801.
- [11] G. Rehman, et al., Electronic band structures of the highly desirable III–V semiconductors: TB-mBJ DFT studies, *J. Electron. Mater.* 45 (2016) 3314–3323.
- [12] Y. Liang, G. Shao, First principles study for band engineering of  $\text{KNbO}_3$  with 3d transition metal substitution, *RSC Adv.* 9 (13) (2019) 7551–7559.
- [13] J. Cao, et al., Defects and dopants in zinc-blende aluminum arsenide: a first-principles study, *New J. Phys.* 23 (1) (2021) 013018.
- [14] D. Bolger, B. Barry, Preparation of aluminium arsenide by a vapour phase transport reaction, *Nature* 199 (4900) (1963), 1287–1287.
- [15] R. Kopf, et al., N-and P-type dopant profiles in distributed Bragg reflector structures and their effect on resistance, *Appl. Phys. Lett.* 61 (15) (1992) 1820–1822.
- [16] B. Davidson, et al., The lattice sites of carbon in highly doped AlAs: C grown by molecular beam epitaxy, *Semicond. Sci. Technol.* 8 (4) (1993) 611.

- [17] B. Koiller, X. Hu, S.D. Sarma, Exchange in silicon-based quantum computer architecture, *Phys. Rev. Lett.* 88 (2) (2001) 027903.
- [18] R. Yang, et al., A first-principles study of the properties of four predicted novel phases of AlN, *J. Phys. Chem. Solid.* 104 (2017) 68–78.
- [19] J.P. Perdew, et al., Prescription for the design and selection of density functional approximations: more constraint satisfaction with fewer fits, *J. Chem. Phys.* 123 (6) (2005).
- [20] Z. Aboub, B. Daoudi, A. Boukraa, Theoretical study of Ni doping SrTiO<sub>3</sub> using a density functional theory, *AIMS Materials Science* 7 (6) (2020) 902–910.
- [21] S.J. Clark, et al., First principles methods using CASTEP, *Z. für Kristallogr. - Cryst. Mater.* 220 (5–6) (2005) 567–570.
- [22] J.P. Perdew, K. Burke, M. Ernzerhof, Generalized gradient approximation made simple, *Phys. Rev. Lett.* 77 (18) (1996) 3865.
- [23] J.P. Perdew, et al., Restoring the density-gradient expansion for exchange in solids and surfaces, *Phys. Rev. Lett.* 100 (13) (2008) 136406.
- [24] H.J. Monkhorst, J.D. Pack, Special points for Brillouin-zone integrations, *Phys. Rev. B* 13 (12) (1976) 5188.
- [25] W. Holzappel, Equations of state for solids under strong compression, *Z. für Kristallogr. - Cryst. Mater.* 216 (9) (2001) 473–488.
- [26] J. Sun, A. Ruzsinszky, J.P. Perdew, Strongly constrained and appropriately normed semilocal density functional, *Phys. Rev. Lett.* 115 (3) (2015) 036402.
- [27] F.D. Murnaghan, The compressibility of media under extreme pressures, *Proc. Natl. Acad. Sci. USA* 30 (9) (1944) 244–247.
- [28] S. Adachi, *Properties of Semiconductor Alloys: Group-IV, III-V and II-VI Semiconductors*, John Wiley & Sons, 2009.
- [29] M. Faizan, et al., First-principles study of the double perovskites Sr<sub>2</sub>XO<sub>6</sub> (X= Li, Na, Ca) for spintronics applications, *Bull. Mater. Sci.* 39 (2016) 1419–1425.
- [30] O. Nemiri, et al., *J. Mol. Graph. Model.* 92 (2019), 140e146.
- [31] K. Panda, K.R. Chandran, First principles determination of elastic constants and chemical bonding of titanium boride (TiB) on the basis of density functional theory, *Acta Mater.* 54 (6) (2006) 1641–1657.
- [32] S.K. Manjeshwar, *Free-Space Cavity Optomechanical Systems on a Chip with III-V Heterostructures*, Chalmers Tekniska Hogskola, (Sweden), 2023.
- [33] J. Den Toonder, J. Van Dommelen, F. Baaijens, The relation between single crystal elasticity and the effective elastic behaviour of polycrystalline materials: theory, measurement and computation, *Model. Simulat. Mater. Sci. Eng.* 7 (6) (1999) 909.
- [34] A. Najim, et al., Theoretical investigation of structural, electronic, and optical properties of halide cubic perovskite CsPbBr<sub>3</sub>-xI<sub>x</sub>, *Mater. Sci. Semicond. Process.* 141 (2022) 106442.
- [35] D. Pettifor, Theoretical predictions of structure and related properties of intermetallics, *Mater. Sci. Technol.* 8 (4) (1992) 345–349.
- [36] S. Pugh, XCII. Relations between the elastic moduli and the plastic properties of polycrystalline pure metals, *London, Edinburgh Dublin Phil. Mag. J. Sci.* 45 (367) (1954) 823–843.
- [37] A. Carvalho, et al., A hybrid density functional study of lithium in ZnO: stability, ionization levels, and diffusion, *Phys. Rev. B* 80 (19) (2009) 195205.
- [38] G.S. Gautam, E.A. Carter, Evaluating transition metal oxides within DFT-SCAN and SCAN+ U frameworks for solar thermochemical applications, *Phys. Rev. Mater.* 2 (9) (2018) 095401.
- [39] N. Rössler, K. Kotsis, V. Staemmler, Ab initio calculations for the Zn 2s and 2p core level binding energies in Zn oxo compounds and ZnO, *Phys. Chem. Chem. Phys.* 8 (6) (2006) 697–706.
- [40] P. Blaha, et al., wien2k, An Augmented Plane Wave+ Local Orbitals Program for Calculating Crystal Properties 60 (1) (2001).
- [41] F. Tran, P. Blaha, Accurate band gaps of semiconductors and insulators with a semilocal exchange-correlation potential, *Phys. Rev. Lett.* 102 (22) (2009) 226401.
- [42] [https://www.researchgate.net/publication/232417181\\_Band\\_parameters\\_for\\_III-V\\_compound\\_semiconductors\\_and\\_their\\_alloys](https://www.researchgate.net/publication/232417181_Band_parameters_for_III-V_compound_semiconductors_and_their_alloys).
- [43] M. Moin, et al., First-principle calculations to investigate structural, electronic, mechanical, optical, and thermodynamic features of promising (La, In)-doped AlSb for optoelectronic applications, *J. Mol. Model.* 29 (7) (2023) 219.
- [44] R.J. Bushby, S.M. Kelly, M. O'Neill, *Liquid Crystalline Semiconductors: Materials, Properties and Applications*, vol. 169, Springer Science & Business Media, 2012.
- [45] A. Kuzmich, et al., Signal velocity, causality, and quantum noise in superluminal light pulse propagation, *Phys. Rev. Lett.* 86 (18) (2001) 3925.
- [46] M. Jiang, et al., First-principles study of point defects in GaAs/AlAs superlattice: the phase stability and the effects on the band structure and carrier mobility, *Nanoscale Res. Lett.* 13 (2018) 1–13.
- [47] M.A. Ali, et al., First principles study of Cu based delafossite transparent conducting oxides CuXO<sub>2</sub> (X= Al, Ga, in: B. La, Y.) Sc (Eds.), *Materials Science in Semiconductor Processing*, vol. 38, 2015, pp. 57–66.
- [48] C. Ambrosch-Draxl, J.O. Sofo, Linear optical properties of solids within the full-potential linearized augmented planewave method, *Comput. Phys. Commun.* 175 (1) (2006) 1–14.
- [49] **Properties of Semiconductor Alloys: Group-IV, III-V and II-VI Semiconductors. (No Title).**
- [50] G. Murtaza, I. Ahmad, First principle study of the structural and optoelectronic properties of cubic perovskites CsPbM<sub>3</sub> (M= Cl, Br, I), *Phys. B Condens. Matter* 406 (17) (2011) 3222–3229.
- [51] Z. Hussain, et al., Temperature-dependent angle-resolved X-ray photoemission study of the valence bands of single-crystal tungsten: evidence for direct transitions and phonon effects, *Phys. Rev. B* 22 (8) (1980) 3750.
- [52] M.A. Rahman, M.Z. Rahaman, M.A. Rahman, The structural, elastic, electronic and optical properties of MgCu under pressure: a first-principles study, *Int. J. Mod. Phys. B* 30 (27) (2016) 1650199.
- [53] R. Reddy, et al., Correlation between optical electronegativity and refractive index of ternary chalcopyrites, semiconductors, insulators, oxides and alkali halides, *Opt. Mater.* 31 (2) (2008) 209–212.
- [54] M. Fox, *Optical Properties of Solids-AAPT*, Cambridge University Press, New York, 2002.
- [55] A. Delin, et al., Optical properties of the group-IVB refractory metal compounds, *Phys. Rev. B* 54 (3) (1996) 1673.
- [56] C. Chang, et al., Recent progress on two-dimensional materials, *Acta Phys. Chim. Sin.* 37 (12) (2021) 2108017.
- [57] W. Moore, R. Holm, Infrared dielectric constant of gallium arsenide, *J. Appl. Phys.* 80 (12) (1996) 6939–6942.
- [58] M. Dadsetani, A. Pourghazi, Optical properties of strontium monochalcogenides from first principles, *Phys. Rev. B* 73 (19) (2006) 195102.
- [59] D.L. Poster, et al., Ultraviolet radiation technologies and healthcare-associated infections: standards and metrology needs, *J. Res. National Instit. Stand. Technol.* 126 (2021) 1–33.
- [60] F. Tran, WIEN2k: An Augmented Plane Wave Plus Local Orbitals Program for Calculating Crystal Properties, 2018.
- [61] M. Alouani, L. Brey, N. Christensen, Calculated optical properties of semiconductors, *Phys. Rev. B* 37 (3) (1988) 1167.
- [62] B. Arnaud, M. Alouani, Local-field and excitonic effects in the calculated optical properties of semiconductors from first-principles, *Phys. Rev. B* 63 (8) (2001) 085208.
- [63] R. Fern, A. Onton, Refractive index of AlAs, *J. Appl. Phys.* 42 (9) (1971) 3499–3500.
- [64] M.A. Ali, et al., First-principles calculations of opto-electronic properties of IIIs (III= Al, Ga, In) under influence of spin-orbit interaction effects, *Bull. Mater. Sci.* 42 (1) (2019) 36.
- [65] M. Guemou, et al., Ab initio study of the structural, electronic and optical properties of BAs and BN compounds and BNxAs<sub>1-x</sub> alloys, *Phys. B Condens. Matter* 436 (2014) 33–40.
- [66] T. Osotchan, et al., Electronic band structure of Al<sub>x</sub>Ga<sub>1-x</sub>As/Al<sub>y</sub>Ga<sub>1-y</sub>As/GaAs double-barrier superlattices, *Phys. Rev. B* 50 (4) (1994) 2409.
- [67] A.H. Reshak, Z. Charifi, H. Baaziz, First-principles study of the optical properties of PbFX (X= Cl, Br, I) compounds in its matlockite-type structure, *Eur. Phys. J. B* 60 (2007) 463–468.